Soft Matter

Cite this: *Soft Matter*, 2012, **8**, 8896

www.rsc.org/softmatter

PAPER

Non-amphiphilic pyrene cored poly(aryl ether) dendron based gels: tunable morphology, unusual solvent effects on the emission and fluoride ion detection by the self-assembled superstructures†

P. Rajamalli and Edamana Prasad*

Received 18th May 2012, Accepted 27th June 2012
DOI: 10.1039/c2sm26151k

The design, synthesis and study of morphology as well as photophysical properties of novel low molecular weight gels (LMWG) based on non-amphiphilic pyrene cored poly(aryl ether) dendron derivatives are described. Solvent controlled self-assembly in the system results in nano-sized vesicles, which further aggregate to micro-sized vesicles and finally turned to entangled fibrillar type arrangement in the gel phase. The morphology transformations were investigated by dynamic light scattering (DLS), scanning electron microscopy (SEM), transmission electron microscopy (TEM), atomic force microscopy (AFM) and confocal laser scanning microscopy (LSCM) experiments. The nano-/micro-sized vesicles and fibre aggregates exhibit an intense light emitting property from the pyrene moiety, which is attached to the dendron through an acylhydrazone spacer group. More interestingly, the luminescence properties were found to be controlled by the solvent polarity, in a rather unusual manner, due to the selective formation of pyrene 'excimer' and 'exciplex' in solvent controlled aggregates. Furthermore, the system has been utilized to detect fluoride ions through a reversible gel–sol transition, which is associated with a color change from yellow to red.

Introduction

In the recent past, low-molecular-mass organic gelators (LMOGs) containing polycyclic aromatic hydrocarbons have gained considerable attention due to their potential role in various optoelectronic devices for enhanced charge transport and emission intensity.[1–5] Designing LMOGs with attractive fluorescence properties is highly desirable in the context of developing functional materials for sensing and imaging applications.[6] Study of the self-assembly of fluorescent LMOGs to various nano-architectures is vital in nanoscience and technology, particularly in the emerging fields of supramolecular electronics.[7–9] Among the varied shapes generated by the molecular assembly, *micelles*, *fibres* and *vesicles* have gathered much interest since they are important three-dimensional molecular assemblies for biomimetics study, functional nanomaterials, resonance energy transfer study and building drug and gene delivery systems.[10–22] While a large number of amphiphilic polymers and surfactants are known to spontaneously form vesicles,[23–28] only limited examples are available in the literature for non-amphiphilic structures forming vesicles. For example, elegant works by Ajayaghosh and co-workers have demonstrated the formation of fluorescent vesicles from non-amphiphilic oligomer structures.[29,30] In another interesting study, Li *et al.* have described vesicle formation by oligomers and foldamers, which are non-amphiphilic in nature.[31,32]

Dendrimers are macromolecules with well-defined architectures and flexible molecular framework at the nanoscale.[33–36] Our continued interest in the design and utilization of dendrimer based low-molecular-mass organogels[37,38] prompted us to develop organogels with 'tunable' morphology and light emitting properties. While amphiphilic and zwitterionic dendrimers/dendrons forming flexible morphology are known in the literature,[39,40] *non-amphiphilic* type dendrimers/dendrons, which spontaneously self-assemble to various morphologies, have not been reported so far. Herein, we describe the controlled formation of nano- to micrometer-sized *vesicles* and *fibres* from *non-amphiphilic* pyrene cored poly(aryl ether) dendrons. To the best of our knowledge, this is the first report on developing a fluorescent organogel based on a *non-amphiphilic* poly(aryl ether) dendron derivative which exhibits 'vesicle' as well as 'fibre' morphology. We have also investigated the role of solvent polarity on the morphology and photophysics of the system and the results reveal an unusual solvent dependency on the emission wavelength from the self-assembled system. Furthermore, the ability of the system to detect anions such as fluoride ions has been analysed.[6d]

Department of Chemistry Indian Institute of Technology Madras (IITM), Chennai, 600036, India. E-mail: pre@iitm.ac.in; Fax: +91 44-2257-4202

† Electronic supplementary information (ESI) available: Synthetic procedure, characterization methods, SEM, TEM, AFM images, Jobs plot, CD spectrum, *etc.* See DOI: 10.1039/c2sm26151k

Results and discussion

Gel formation

The first and second generations (G1 and G2, respectively) of AB_2 and AB_3 type poly(aryl ether) dendrons containing pyrene moiety, attached through an acylhydrazone spacer unit, were synthesized based on a reported procedure (Fig. 1).[38] Pyrene fluorophore was selected since its derivatives have been well recognized and extensively utilized in designing biological probes, artificial light-harvesting systems, photonic devices and organic semiconductors.[41–44]

Compounds **I** to **IV** are sparingly soluble in moderately polar solvent environments (Table 1), under ambient conditions. However, the compounds were dissolved completely by heating followed by sonication for three to four minutes. The system suddenly turned to gel upon cooling to room temperature. The critical gel concentration (CGC) values of the compounds were determined in each solvent and are given in Table 1. In order to analyse the solvent effect on the gelation properties quantitatively, we correlate the CGC values of the gelator with the solvent parameters such as dielectric constant (ε), Reichardt's parameter (E_T), and the Kamlet–Taft parameter.[45] A plot of dielectric constant *vs.* CGC values of the compounds (Fig. S1a†) does not provide a definite correlation, indicating that the dielectric constant of solvents does not play a significant role in controlling the specific solute–solvent interactions at the molecular level. A similar trend is observed for the mixture of solvents examined in this study. For example, the CGC values for compound **IV** did not vary drastically in a mixture of chloroform (ε-4.8) and methanol (ε-32.7), compared to that of chloroform and hexane (ε-1.9), even though the dielectric constant of the solvent mixtures is expected to be distinct. We have also analyzed the role of solvent polarity parameter (Reichardt's parameter, E_T) on the gelation properties of the compounds described. Fig. S1b† depicts the variation of CGC with respect to the E_T values of different solvents. The plot shows a weak correlation between solvent polarity parameter and CGC values. The Reichardt's parameter for the mixture of chloroform (E_T -39.1) and methanol (E_T -55.4) is expected to be higher than that of the mixture of chloroform and hexane (E_T -31.4). Since the CGC values of the gelators are not varied between the two different solvent mixtures mentioned above, we conclude that polarity has a poor role in regulating specific solute–solvent interaction at the molecular level.[45a] We then compared the effect of solvents on gelation ability in terms of Kamlet–Taft parameters, where solvents are described in terms of their ability to donate (α), accept (β) hydrogen bonds and generalized polarity parameter (π^*). Similar to the above-mentioned cases, a weak correlation between Kamlet–Taft parameters and CGC values was observed as shown in Fig. S2a and c.† Kamlet–Taft parameters vary widely from polar solvents such as methanol (α-0.98, β-0.66, π^*-0.60) to non-polar solvents such as hexane (α-0.00, β-0.00, π^*-0.04) and comparable CGC values in chloroform–methanol and chloroform–hexane mixtures suggest that the parameters appear to be less important in the present case. The trend remains identical for all the gelators examined in the study.

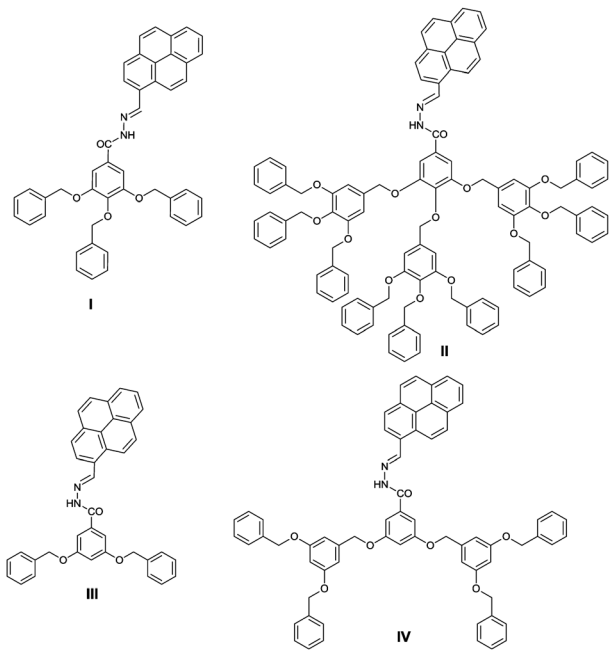

Fig. 1 Structure of the compounds used in the present study.

The CGC value provides another pathway to understand the correlation between gelator action and gelator solubility. From Table 1, it is clear that gelators show relatively high CGC values in single solvents like $CHCl_3$, THF, dioxane, DMF, *etc.*, compared to solvent mixtures due to the high solubility of the gelators in these solvents. However, slight decreases in the CGC values are observed in the presence of highly polar (methanol or water) or highly non-polar (hexane) solvents, which is likely due to the fact that the presence of poor solvents provides improved π–π interactions in the system.[45c] AB_2 type poly(aryl ether) dendrons form gel in several organic solvents at very low CGC values. The propensity of gel formation by compounds **III** and **IV** (AB_2 type) was high compared to that of compounds **I** and **II** (AB_3 type). This can be attributed to the steric hindrance in compounds **I** and **II** due to the increased number of benzyl units which disrupts the planarity of the molecules and their self-assembly.

The FT-IR spectrum of gel **IV** (from $CHCl_3$) shows a single amide (C=O) stretching vibration band at 1641 cm^{-1} and an intense NH stretching vibration at 3189 cm^{-1} (Fig. S3†). This is an unambiguous signature of the presence of a network of hydrogen-bonded amides. In addition to this evidence, powder XRD patterns of the compounds **I** to **IV** exhibit a reflection peak in the wide-angle region, which is characteristic of a typical π–π stacking distance in the range of 3.42–3.59 Å (Fig. S4a to d†), indicating that hydrogen bonding and π–π stacking interactions hold the self-assembled system in the gel phase. The gel transition temperature increases as the concentration of the gel increases and Fig. S5† shows the linear relation between the gel transition temperature (53–63 °C) and the corresponding gel concentration (0.2–1.2 wt%) for the first generation AB_2 type dendron derivatives in a THF–water mixture (1 : 1).

Tunable morphology

The morphology of the xerogels of the dendron derivatives in chloroform was examined by scanning electron microscopy

Table 1 Gelation properties and critical gel concentrations (CGCs) of dendrons in various organic solvents and mixture of solvents at 25 °C[a]

Medium	I	II	III	IV
$CHCl_3$	P.G	G(5.5)	G(6)	G(4)
DCM	P.G	G(6)	G(7)	G(5)
THF	G(8)	G(4)	G(5)	G(4)
Dioxane	G(9)	G(7)	G(6.5)	G(9)
Acetone	G(5)	G(4)	G(3.5)	G(5)
DMF	G(15)	G(12)	G(20)	G(25)
Ethyl acetate	G(8)	(3)	G(5)	T.G(4)
Pyridine	G(4)	S	G(5)	S
Ethanol	I	I	I	I
Toluene	P.G	G(10)	P.G	T.G(6)
Acetonitrile	G(3.5)	G(10)	G(5)	G(15)
Acetophenone	G(11)	G(6)	G(9)	G(4)
DMF : water	G(4) (1 : 1)	G (6) (1 : 1)	G(6) (1 : 1)	G(5) (1 : 1)
THF : water	G(4) (1 : 1)	G(3.5) (1 : 1)	G(3.5) (1 : 1)	G(3) (1 : 1)
Dioxane : water	G(5) (1 : 1)	G(7) (1 : 1)	G(6) (1 : 1)	G(8) (1 : 1)
$CHCl_3$: methanol	P.G	G(4) (1 : 1)	P.G	G(3.5) (1 : 1)
$CHCl_3$: hexane	P.G	G(3.5) (1 : 1)	G(4) (1 : 1)	G(3) (1 : 1)

[a] The value given in parentheses is the CGC in mg ml^{-1}. For solvent mixtures, the ratio is also given in parentheses. G = Gel, T.G = Transparent gel, S = Solution, P.G = Partial gel, I = Insoluble.

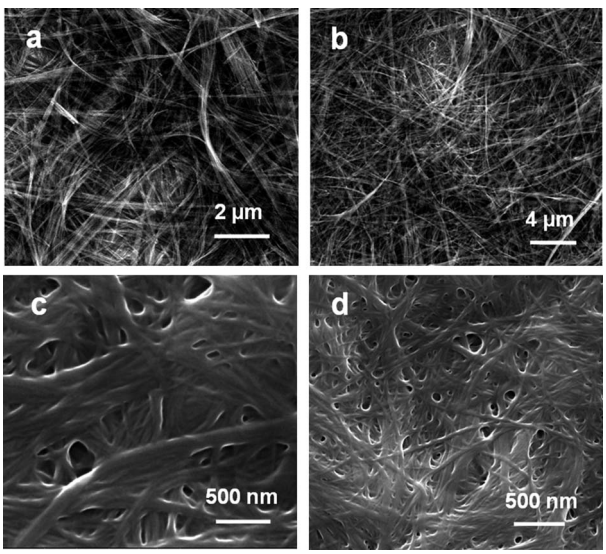

Fig. 2 SEM images of xerogel formed from first generation compounds **I** and **III** (a and b, respectively) and second generation compounds **II** and **IV** (c and d, respectively).

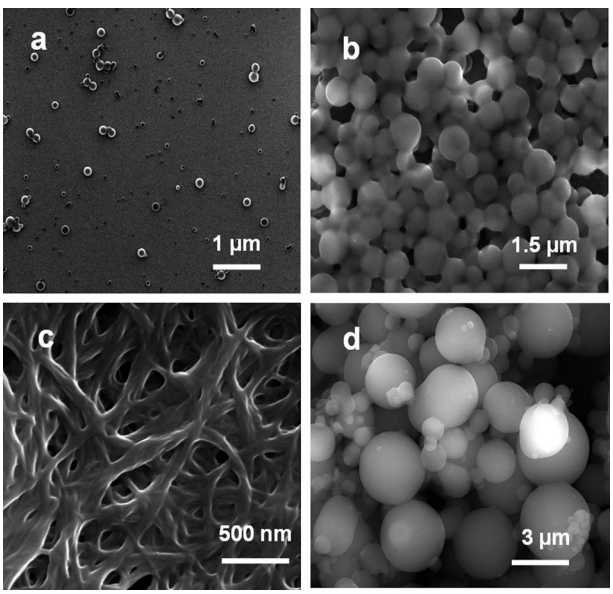

Fig. 3 SEM images of xerogel formed from compound **IV** in $CHCl_3$–MeOH at (a) 1×10^{-5} M, (b) 1×10^{-4} M, and (c) 3.5×10^{-3}; (d) SEM image of compound **IV** (1×10^{-4} M) in $CHCl_3$–hexane.

(SEM). The SEM images are shown in Fig. 2. The four gelators form nano-fibrillar type arrangement, where the thickness of the fibres was relatively higher in the first generation dendrons, compared to that formed from the second generation.

The morphology of the xerogels of the dendron derivatives formed from varied solvent mixtures was also examined by SEM. While all the compounds exhibit fibrillar type assembly in single solvents, fine-tuning of the polarity of the medium resulted in the formation of spherical morphology in the system. Initial experiments were carried out in $CHCl_3$–MeOH (relatively polar) and $CHCl_3$–hexane (relatively non-polar) mixtures. The results from SEM studies suggest that compounds **II** and **IV** (second generation) form well defined nano-spheres with a diameter range of 200–300 nm at concentrations below CGC (1×10^{-5} M) (Fig. 3a). Upon increasing the concentrations by an order of magnitude (1×10^{-4} M), the nano-spheres fuse together resulting in the formation of microspheres. Interestingly, the size of the microsphere exhibited a solvent dependency. While the average diameter of 1 μm was obtained for the microspheres in a $CHCl_3$–MeOH mixture, an increased diameter of 3 μm was obtained in a $CHCl_3$–hexane mixture (Fig. 3b and c). The SEM images clearly reveal that the initially formed nano-sphere assembly could further combine to generate twins, triplets or even multiplets, suggesting that larger structures were formed by the fusion of the smaller ones (see Fig. S6a†). The microspheres can further self-assemble to form extended structures (nanofibres) in solvent mixtures at concentrations above CGC (>1×10^{-3} M, Fig. 3d and S6c†). The tunable morphology was, however, not observed in the first generation dendrons (compounds **I** and **III**) where

predominantly nano-fibres were formed in solvent mixtures over a wide range of concentrations (Fig. S6d†). The generation dependency on the aggregate morphology indicates that the conformational flexibility adopted by the system is crucial in deciding the final self-assembled structure.

In order to verify whether drying results in significant changes in the initial morphology of the aggregates, dynamic light scattering (DLS) experiments were carried out at lower (10^{-5} M) and higher (1×10^{-4} M) concentrations of compounds **II** and **IV** in a $CHCl_3$–MeOH mixture. DLS studies carried out at the lower concentration range indicate the presence of aggregates having distributions of varying hydrodynamic diameters, with a mean diameter (D_h) of 200–300 nm (Fig. S7†). At a relatively higher concentration range, the hydrodynamic diameter exhibited a mean diameter (D_h) of 1.0–1.3 μm. The results are strikingly consistent with the SEM analysis described above indicating that microscopic images reflect actual morphology of the aggregated systems. The values of the hydrodynamic diameter also suggest that the microspheres formed were vesicles and not micelles, since the diameter for micellar structures would normally fall in the range of 3–7 nm.[46]

Next, atomic force microscopic images were taken for compounds **I** to **IV** in chloroform. The nano-sized fibres in the gel systems were evident in the AFM images and average height of the fibres was found to be 200 nm and 40 nm for generations **I** and **II**, respectively (Fig. S8a and d†). AFM images of **II** and **IV** were also investigated in the mixture of solvents to get more insight into the morphology of the initially formed nano-/micrometer assemblies and the subsequent transformation to superstructures (Fig. 4 and S9†). The ratio of the diameter to the height of the assembly was estimated to be 4 nm for the case of compound **IV**, indicating that the soft structures are flattened after transferring from the solution phase to silicon wafer. This can be attributed partially to the slow evaporation of the solvent molecules from the assembly and/or to the high local force applied by the AFM tip. Surprisingly, the AFM images of the dendron derived gels (**I–IV**) from toluene indicate the presence of a one dimensional helical network structure and spiral nano-fibre formation (Fig. 4b and S10†). The AFM images indicate that the widths of these helical fibres are within the range of 80–110 nm. The morphology of the single helix is shown to be twisted with a left- and right-handed pattern and the helical pitches vary from 100–170 nm. Furthermore, left- and right-handed helical fibres were present in equal quantities, thus resulting in overall racemic mixtures without any CD signals (for example, see Fig. S11†). While the elegant work by Percec *et al.* demonstrated the self-assembly and formation of helical structures from achiral dendrons, formation of helical gel systems from achiral poly(aryl ether) dendrons has not been reported yet.[47,48]

The hollow feature of the vesicle was confirmed by fluorescence microscopy images (Fig. 5) where there is a large difference in the luminescence of the outer ring relative to that of the inner areas. This clearly shows that vesicles are centrally hollow and filled with fluorescent-silent solvent molecules. To our surprise, the vesicles exhibited two different fluorescent colors in $CHCl_3$–MeOH and $CHCl_3$–hexane mixtures (blue and green, respectively) (*vide infra*).

To further examine the morphology, TEM images of the compounds **I** to **IV** were taken from single solvents. The images show nano-fibre formation, consistent with the SEM analysis (Fig. S12a to d†). The TEM images for compounds **II** and **IV** were also taken from a mixture of solvents and the images revealed the hollow feature of the vesicles (Fig. 6). The magnified TEM images (Fig. S13†) suggest that the wall thickness of the vesicles of compound **IV** was *ca.* 6 nm when the gel is formed from a $CHCl_3$–hexane mixture and 3.1 nm when the gel is formed from a $CHCl_3$–MeOH mixture (Fig. S13†). The vesicle to fibre transformation by the dendron derivatives was further confirmed through TEM images (see Fig. 6b), where the fusion of initially formed vesicles is clearly observed.

Fluorescence properties

Although the poly(aryl ether) dendron derivatives are non-fluorescent in the solution phase (<10^{-4} M in single solvents and

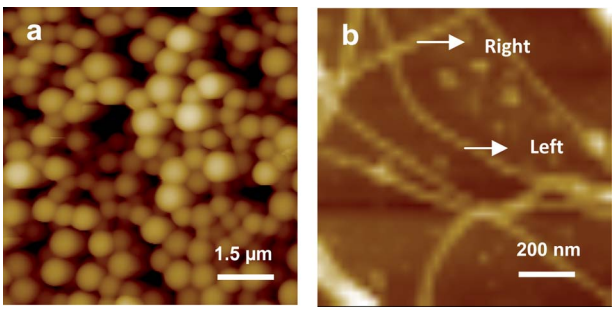

Fig. 4 AFM images of compound **IV**: (a) vesicles formed in $CHCl_3$–MeOH (1×10^{-4} M) and (b) helical fibres formed in toluene at room temperature.

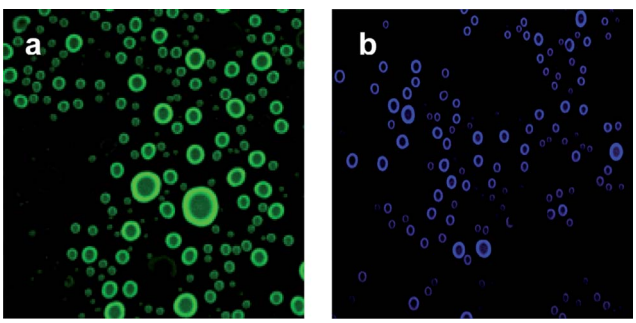

Fig. 5 LSCM images of vesicles formed from compound **IV** (1×10^{-4} M) (a) in $CHCl_3$–hexane and (b) in $CHCl_3$–MeOH at room temperature.

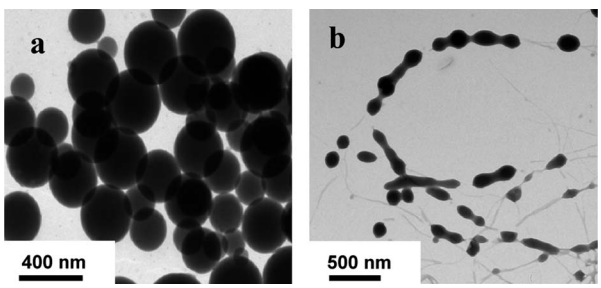

Fig. 6 TEM images of compound **IV** in $CHCl_3$–MeOH (1×10^{-5} M) at room temperature: (a) vesicle formation and (b) fusion of vesicles.

$<10^{-6}$ M in solvent mixtures), enhanced emission was observed from all the compounds under aggregated conditions. For example, Fig. 7 shows the photographs of compound **IV** in chloroform (1×10^{-4} M) and the gel phase, under visible and UV illumination. It is evident that there is no emission from the solution phase under UV and visible light excitation. Nonetheless, the gel formation resulted in bright green emission under UV light (Fig. 7).

The fluorescence intensity from the gel phase was enhanced by ~750 fold compared to that in the solution phase (Fig. 8a). The remarkable fluorescence enhancement from the gel systems can be explained by gel-induced enhanced emission (GIEE).[49] The enhanced emission from the remaining compounds (**I–III**) is shown in the ESI (Fig. S14†). Laser scanning confocal microscopy (LSCM) was utilized to obtain the images of the fluorescing gels through drop casting on a microscope coverslip. The confocal microscopic image of compound **IV** is given in Fig. 8b which reveals the presence of a dense 3D network of greenish fluorescent fibres.

The structureless features of the luminescence emission from the gel systems (λ_{max} = 520–530 nm) suggest that the emission is from pyrene excimer. The excited state luminescence lifetime of the gels was measured and the fluorescence decays were best fit for a triexponential curve with 9.46 ns (65.85%), 2.41 ns (17.33%) and 0.43 ns (16.82) (Fig. S15†) and the highest lifetime value is attributed to the pyrene excimer emission.[50]

Role of solvent in 'tuning' the emission

Since solvent polarity can control the size and morphology of the self-assembled systems described, we hypothesized that the solvent milieu could affect the emission properties from the gel systems. The experimental result suggests that there is an unconventional solvent dependent wavelength shift for the emission. For example, upon exciting the gel formed in a $CHCl_3$–MeOH mixture at 410 nm, a broad structureless band is observed around 445 nm, associated by a bright-blue emission. In contrast, a broad structureless bright-green emission is observed from the gel around 525 nm in a relatively more non-polar environment ($CHCl_3$–hexane mixture). The emission maximum from the gel in toluene was, however, in between (470 nm). Fig. 9 depicts the emission spectra of compound **IV** in the gel formed from varied solvents. The corresponding spectra for compound **II** is given in the ESI (Fig. S14d†).

These results are quite unexpected since the shift in the emission wavelength is independent of solvent polarity, suggesting that the role of the solvent in controlling the photophysics of the self-assembly of the dendron systems is subtle (*vide infra*).

Mechanism of the self-assembly

Results taken together suggest that gelation in generation **I** dendrons always leads to fibre type self-assembled structures irrespective of the solvent milieu and concentrations. The self-assembly might occur through a two-step hierarchical supramolecular mechanism, as we have observed in the corresponding anthracene analogues.[38] First, the molecules are assembled through hydrogen bonding and π–π interactions into one-dimensional extended assemblies, followed by intertwining of the chains to form the elementary fibre. However, the morphological features of the generation **II** dendrons in the present study are remarkably different from the anthracene cored dendron analogues.[38]

In a polar environment, the acylhydrazone spacer group is likely to be exposed to a solvent medium, and the appended benzyl rings as well as pyrene groups could 'fold back' due to hydrophobic interactions. The self-assembly of such folded dendrons results in the formation of vesicles in which pyrene and benzene units are placed at close proximity and this can potentially lead to exciplex formation upon photoexcitation.[51] This is consistent with the blue emission obtained from the LSCM images and the emission spectra of the second generation dendron derivatives. On the other hand, it is likely to have predominantly π–π stacking interaction between pyrene

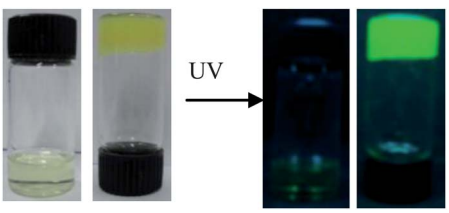

Fig. 7 Photographs of compound **IV** in chloroform (1×10^{-4} M) and in the gel phase under ambient light (left) and under UV illumination (right).

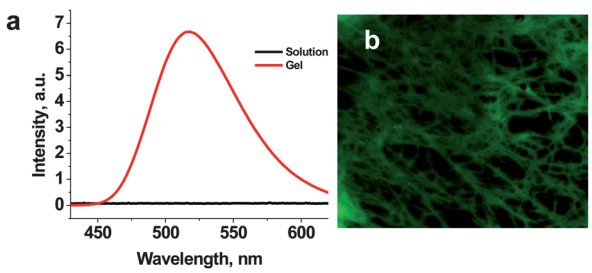

Fig. 8 (a) Emission spectra of compound **IV** in the gel phase (red) and in chloroform solution (1×10^{-4} M) (black); (b) LSCM image of the gel formed from compound **IV** in $CHCl_3$ at room temperature.

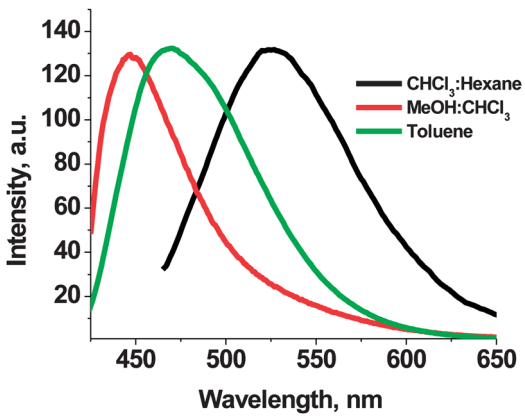

Fig. 9 Emission spectra of compound **IV** (gel) formed from varied solvent environments.

moieties during the self-assembly of the dendron derivatives in a relatively less polar solvent, resulting in the formation of pyrene excimer, upon photoexcitation. This is consistent with the observation of the green emission from the second generation dendron derivatives in a $CHCl_3$–hexane mixture. The third type of emission was observed at 470 nm in toluene. This can be attributed to the pyrene excimer emission, where the pyrene units are partially overlapped in the excited state, due to the helical type of self-assembly.[52] Based on the photophysical results, a schematic representation of the above-mentioned processes is proposed in Fig. 10.

As a corollary of the solvent dependent self-assembly, we expect a difference in the wall thickness of the vesicle formed in different solvent environments. The space-filling model of compound **IV** in the energy minimized structure showed 1.6 nm as the distance between the spacer group and the end groups, implying that the folded double layer self-assembly of compound **IV** would have a total length of 3.1 nm (path b in Fig. 10). This is strikingly consistent with the results obtained from the TEM analysis where the wall thickness of the vesicles in a chloroform–methanol mixture was found to be 3.1 nm (Fig. S13†). Similarly, the end to end distance for an extended structure of compound **IV** was 3.1 nm. This is also concurrent with the wall thickness obtained from TEM analysis (6 nm), where two such units were self-assembled in a linear fashion (path a in Fig. 10). The results suggest that the vesicles have a double layer outer surface.

Fluoride ion detection

The use of this low molecular weight fluorescent gel as a sensor for various anions (F^-, Cl^-, Br^-, I^-, ClO_4^-, CH_3COO^-, $H_2PO_4^-$ and HSO_4^- as Bu_4N^+ salts) was examined in THF. The gels from compounds **I** to **IV** show intense variation in their electronic absorption spectra *only* upon the addition of tetra-butylammoniumfluoride (TBAF) at room temperature (Fig. S16a to c†). The presence of F^- ions not only changes the color of the systems, but also disrupts the preformed gel into a

Fig. 11 Photographs of (i) organogel formed from compound **IV** in THF, (ii) after addition of TBAF (1 equiv.), and (iii) after addition of water (0.2 ml).

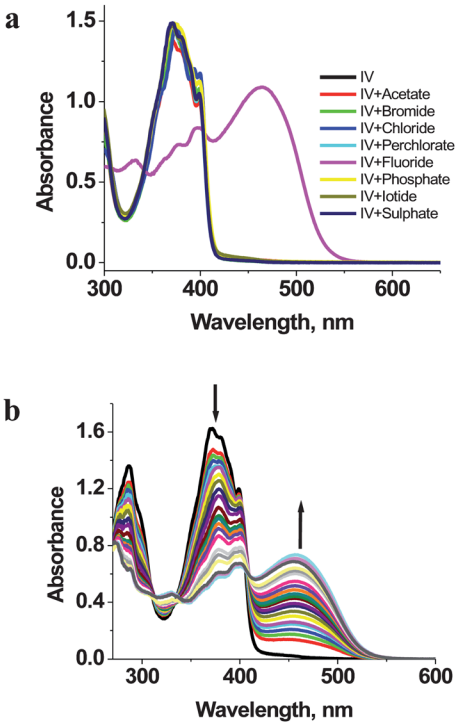

Fig. 12 (a) UV-vis absorption spectra of compound **IV** (5×10^{-5} M) in the presence of 1 equiv. of various anions in THF and (b) increasing the concentration of the fluoride ion (0.01–1 equiv.).

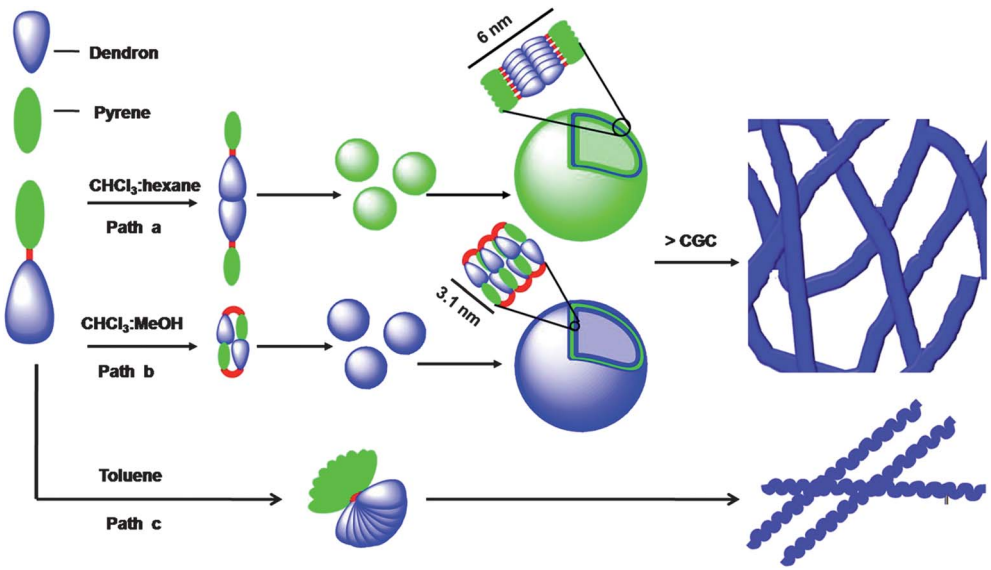

Fig. 10 Scheme representing different types of self-assembly of the dendrons to form a gel.

solution through slow diffusion of the anion. The photographs of the fluoride induced gel-to-sol conversion are given in Fig. 11. The drastic color change of the gels due to the addition of fluoride ions reflects the significant changes in the electronic structure of the system. The UV-vis absorption spectra of compounds **I–IV** in THF (5×10^{-5} M) in the presence of 1 equiv. of various anions were taken at room temperature (Fig. 12 and S16a and c†). As is clear from the figures, the absorption band of compounds **I–IV** is shifted to a longer wavelength only in the presence of fluoride ions.

The evidence for the reaction mechanism was obtained from ^{1}H NMR experiments in DMSO-d_6 (Fig. S17†). Before addition of F^- ions, the ^{1}H NMR chemical shift values of –CH=N– and –NH protons in the compounds were at 9.65 and 12.05 ppm, respectively. After addition of 1 equivalent of F^- ions, the NH signal disappeared which suggested that the NH groups underwent a deprotonation reaction.[38]

Conclusions

In summary, we have initiated the synthesis, morphology study and photophysics of *non-amphiphilic* poly(aryl ether) dendron based tunable fluorescent gel systems. The gels exhibit controlled size and morphology, induced by concentration and solvent polarity. While the second generation dendrons form nano- and micro-sized vesicles below CGC, giant fibrillar type assemblies are formed above CGC. The self-assembly was associated with a ~750 fold enhancement in emission intensity compared to that of solution. Importantly, the gel system exhibited unconventional solvent effects on emission wavelength, which is attributed to the controlled formation of 'excimer' and 'exciplex' from the pyrene moiety in the self-assembly. The current gel system was also employed to detect F^- ions, resulting in the sol–gel transition with an intense color change from yellow to red.

Experimental section

Materials and equipment

The starting materials were purchased from Sigma-Aldrich Chemical Co. and used without further purification, unless otherwise stated. The synthetic routes and characterization of pyrene cored poly (aryl ether) dendron are described in the Synthesis part and ESI.† ^{1}H and ^{13}C NMR data were collected on a Bruker 400 MHz spectrometer (^{1}H: 400 MHz; ^{13}C: 100 MHz). Mass spectra were recorded using a Micromass Q-TOF mass spectrometer and a Voyager-DE PRO MALDI/TOF mass spectrometer with α-cyano-4-hydroxylcinnamic acid (CCA) as the matrix. The IR spectrum was recorded using a Jasco FT/IR-4100 spectrometer. Luminescence experiments were carried out on a Horiba Jobin Yvon Fluoromax-4 fluorescence spectrophotometer. The fluorescence decay measurements were carried out by the time correlated single-photon counting technique (TCSPC) with a microchannel plate photomultiplier tube (MCP-PMT) as the detector and a picosecond laser as the excitation source (model 5000 U, IBH, UK). The scanning electron microscopic studies were carried out using a FEI-Quanta Microscope. AFM samples were prepared by the spin-coating method on silicon wafer and images were recorded using a Park-system XE-100 in the non-contact mode regime. Powder-XRD patterns were recorded on a Bruker D8 Advance X-ray diffractometer using Cu-Kα radiation ($\lambda = 1.54178$ Å). Dynamic light scattering (DLS) experiments were done on a Malvern Zetasizer nano-series 25 °C, with a path length of 1 cm. The wavelength of the laser used was 632.8 nm and the scattering angle was kept at 90.

Synthesis

A solution of 1-pyrene carboxaldehyde (0.506 g, 0.0022 mole) in methanol was added drop wise to a $CHCl_3$ solution of compound **a** (1 g, 0.0022 mole).[38] The mixture was stirred for 3 hours. The resulting precipitate was filtered off by suction and dried under vacuum to yield **I** (1.45 g, 96.2%). ^{1}H NMR (400 MHz, DMSO-d_6) δ: 5.03 (s, ArCH_2O, 2H), 5.23 (s, ArCH_2O, 4H), 7.26–7.51 (m, Ar*H* & Ph*H*, 17H), 8.11 (t, Py*H*, $J = 7.6$ Hz, 1H), 8.25 (m, Py*H*, 2H), 8.36 (d, Py*H*, $J = 7.6$ Hz, 4H), 8.59 (d, Py*H*, $J = 8$ Hz, 1H), 8.84 (d, Hz, $J = 9.2$ Hz, Py*H*, 1H), 9.49 (s, C*H*=N, 1 H), 11.97 (s, CON*H*, 1H); ^{13}C NMR (100 MHz, DMSO-d_6) δ: 70.08, 74.94, 107.74, 124.31, 124.88, 125.10, 125.29, 125.45, 125.71, 126.89, 127.52, 128.09, 128.20, 128.30, 128.44, 128.72, 128.78, 129.04, 130.69, 131.15, 131.78, 137.78, 138.04, 138.56, 152.01, 152.31, 168.18; HRMS (ES^+): *m*/*z* calcd for $C_{45}H_{34}N_2O_4$: 666.2519 found: 667.2582$[M + H]^+$.

Notes and references

1 A. R. Hirst, B. Escuder, J. F. Miravet and D. K. Smith, *Angew. Chem., Int. Ed.*, 2008, **47**, 8002–8018.
2 B.-K. An, J. Gierschner and S. Y. Park, *Acc. Chem. Res.*, 2012, **45**, 544–554.
3 W.-W. Tsai, I. D. Tevis, A. S. Tayi, H. Cui and S. I. Stupp, *J. Phys. Chem. B*, 2010, **114**, 14778–14786.
4 K. Sugiyasu, N. Fujita and S. Shinkai, *Angew. Chem., Int. Ed.*, 2004, **43**, 1229–1233.
5 S. Y. Ryu, S. Kim, J. Seo, Y.-W. Kim, O.-H. Kwon, D.-J. Jang and S. Y. Park, *Chem. Commun.*, 2004, 70–71.
6 (*a*) P. Mukhopadhyay, Y. Iwashita, M. Shirakawa, S.-i. Kawano, N. Fujita and S. Shinkai, *Angew. Chem., Int. Ed.*, 2006, **45**, 1592–1595; (*b*) K. K. Kartha, S. S. Babu, S. Srinivasan and A. Ajayaghosh, *J. Am. Chem. Soc.*, 2012, **134**, 4834–4841; (*c*) S. Srinivasan, P. A. Babu, S. Mahesh and A. Ajayaghosh, *J. Am. Chem. Soc.*, 2009, **131**, 15122–15123; (*d*) R. Varghese, S. J. George and A. Ajayaghosh, *Chem. Commun.*, 2005, 593–595.
7 A. P. H. J. Schenning and E. W. Meijer, *Chem. Commun.*, 2005, 3245–3258.
8 S. Diring, F. Camerel, B. Donnio, T. Dintzer, S. Toffanin, R. Capelli, M. Muccini and R. Ziessel, *J. Am. Chem. Soc.*, 2009, **131**, 18177–18185.
9 (*a*) X.-J. Wang, L.-B. Xing, W.-N. Cao, X.-B. Li, B. Chen, C.-H. Tung and L.-Z. Wu, *Langmuir*, 2011, **27**, 774–781; (*b*) S. S. Babu, S. Prasanthkumar and A. Ajayaghosh, *Angew. Chem., Int. Ed.*, 2012, **51**, 1766–1776.
10 R. Blumenthal, M. J. Clague, S. R. Durell and R. M. Epand, *Chem. Rev.*, 2003, **103**, 53–69.
11 K. J. C. van Bommel, A. Friggeri and S. Shinkai, *Angew. Chem., Int. Ed.*, 2003, **42**, 980–999.
12 A. Ajayaghosh, C. Vijayakumar, V. K. Praveen, S. S. Babu and R. Varghese, *J. Am. Chem. Soc.*, 2006, **128**, 7174–7175.
13 X. Zhang, Z. Chen and F. Würthner, *J. Am. Chem. Soc.*, 2007, **129**, 4886–4887.
14 A. Ajayaghosh, V. K. Praveen, C. Vijayakumar and S. J. George, *Angew. Chem., Int. Ed.*, 2007, **46**, 6260–6265.
15 S. S. Babu, K. K. Kartha and A. Ajayaghosh, *J. Phys. Chem. Lett.*, 2010, **1**, 3413–3424.
16 V. K. Praveen, S. J. George, R. Varghese, C. Vijayakumar and A. Ajayaghosh, *J. Am. Chem. Soc.*, 2006, **128**, 7542–7550.

17 Q. Chen, D. Zhang, G. Zhang, X. Yang, Y. Feng, Q. Fan and D. Zhu, *Adv. Funct. Mater.*, 2010, **20**, 3244–3251.
18 A. L. Martin, B. Li and E. R. Gillies, *J. Am. Chem. Soc.*, 2009, **131**, 734–741.
19 Y. Zhu, W. Tong and C. Gao, *Soft Matter*, 2011, **7**, 5805–5815.
20 T. M. Allen and P. R. Cullis, *Science*, 2004, **303**, 1818–1822.
21 E. P. Holowka, V. Z. Sun, D. T. Kamei and T. J. Deming, *Nat. Mater.*, 2007, **6**, 52–57.
22 V. Yesilyurt, R. Ramireddy and S. Thayumanavan, *Angew. Chem., Int. Ed.*, 2011, **50**, 3038–3042.
23 Y. Morishima, *Angew. Chem., Int. Ed.*, 2007, **46**, 1370–1372.
24 Y.-X. Xu, G.-T. Wang, X. Zhao, X.-K. Jiang and Z.-T. Li, *Langmuir*, 2009, **25**, 2684–2688.
25 D. E. Discher and A. Eisenberg, *Science*, 2002, **297**, 967–973.
26 M. A. Greenfield, L. C. Palmer, G. Vernizzi, M. O. Cruz and S. I. Stupp, *J. Am. Chem. Soc.*, 2009, **131**, 12030–12031.
27 S.-Y. Kang, B.-S. Seong, Y. S. Han and H.-T. Jung, *Biomacromolecules*, 2003, **4**, 360–365.
28 J. Yang, D. Lévy, W. Deng, P. Keller and M.-H. Li, *Chem. Commun.*, 2005, 4345–4347.
29 A. Ajayaghosh, R. Varghese, V. K. Praveen and S. Mahesh, *Angew. Chem., Int. Ed.*, 2006, **45**, 3261–3264.
30 A. Ajayaghosh, P. Chithra and R. Varghese, *Angew. Chem., Int. Ed.*, 2007, **46**, 230–233.
31 W. Cai, G.-T. Wang, Y.-X. Xu, X.-K. Jiang and Z.-T. Li, *J. Am. Chem. Soc.*, 2008, **130**, 6936–6937.
32 X.-N. Xu, L. Wang and Z.-T. Li, *Chem. Commun.*, 2009, 6634–6636.
33 M. Grayson and J. M. J. Fréchet, *Chem. Rev.*, 2001, **101**, 3819–3868.
34 P. K. Lekha and E. Prasad, *Chem.–Eur. J.*, 2010, **16**, 3699–3706.
35 M. J. Jasmine and E. Prasad, *J. Phys. Chem. B*, 2010, **114**, 7735–7742.
36 P. K. Lekha and E. Prasad, *Chem.–Eur. J.*, 2011, **17**, 8609–8617.
37 P. Rajamalli and E. Prasad, *New J. Chem.*, 2011, **35**, 1541–1548.
38 P. Rajamalli and E. Prasad, *Org. Lett.*, 2011, **13**, 3714–3717.
39 M. Yang, W. Wang, F. Yuan, X. Zhang, J. Li, F. Liang, B. He, B. Minch and G. Wegner, *J. Am. Chem. Soc.*, 2005, **127**, 15107–15111.
40 Q. Chen, Y. Feng, D. Zhang, G. Zhang, Q. Fan, S. Sun and D. Zhu, *Adv. Funct. Mater.*, 2010, **20**, 36–42.
41 T. Otsubo, Y. Aso and K. J. Takamiya, *J. Mater. Chem.*, 2002, **12**, 2565–2575.
42 W.-L. Jia, T. McCormick, Q.-D. Liu, H. Fukutani, M. Motala, R.-Y. Wang, Y. Tao and S. Wang, *J. Mater. Chem.*, 2004, **14**, 3344–3350.
43 A. Okamoto, K. Kanatani and I. Saito, *J. Am. Chem. Soc.*, 2004, **126**, 4820–4827.
44 V. Percec, M. Glodde, T. K. Bera, Y. Miura, I. Shiyanovskaya, K. D. Singer, V. S. K. Balagurusamy, P. A. Heiney, I. Schnell, A. Rapp, H.-W. Spiess, S. D. Hudson and H. Duan, *Nature*, 2002, **419**, 384–387.
45 (*a*) A. R. Hirst and D. K. Smith, *Langmuir*, 2004, **20**, 10851–10857; (*b*) W. Edwards, C. Lagadec and D. K. Smith, *Soft Matter*, 2011, **7**, 110–117; (*c*) A. R. Hirst, I. A. Coates, T. Boucheteau, J. F. Miravet, B. Escuder, V. Castelletto, I. W. Hamley and D. K. Smith, *J. Am. Chem. Soc.*, 2008, **130**, 9113–9121.
46 T. Dwars, E. Paetzold and G. Oehme, *Angew. Chem., Int. Ed.*, 2005, **44**, 7174–7199.
47 V. Percec, A. E. Dulcey, M. Peterca, M. Ilies, S. Nummelin, M. J. Sienkowska and P. A. Heiney, *Proc. Natl. Acad. Sci. U. S. A.*, 2006, **103**, 2518–2523.
48 V. Percec, A. E. Dulcey, V. S. K. Balagurusamy, Y. Miura, J. Smidrkal, M. Peterca, S. Nummelin, U. Edlund, S. D. Hudson, P. A. Heiney, H. Duan, S. N. Magonov and S. A. Vinogradov, *Nature*, 2004, **430**, 764–768.
49 M. K. Nayak, B.-H. Kim, J. E. Kwon, S. Park, J. Seo, J. W. Chung and S. Y. Park, *Chem.–Eur. J.*, 2010, **16**, 7437–7447.
50 Y. Kamikawa and T. Kato, *Langmuir*, 2007, **23**, 274–278.
51 K.-H. Han, E. Lee, J. S. Kim and B.-K. Cho, *J. Am. Chem. Soc.*, 2008, **130**, 13858–13859.
52 B. Adhikari, J. Nanda and A. Banerjee, *Chem.–Eur. J.*, 2011, **17**, 11488–11496.